



Lu–Hf and Re–Os systematics of peridotite xenoliths from Spitsbergen, western Svalbard: Implications for mantle–crust coupling

Sung Hi Choi ^{a,*}, Katsuhiko Suzuki ^b, Samuel B. Mukasa ^c, Jong-Ik Lee ^d, Haemyeong Jung ^e

^a Department of Geology and Earth Environmental Sciences, Chungnam National University, 79 Daehangno, Yuseong-gu, Daejeon 305-764, South Korea

^b Institute for Research on Earth Evolution, Japan Agency for Marine–Earth Science and Technology (JAMSTEC), Yokosuka 237-0061, Japan

^c Department of Geological Sciences, The University of Michigan, 2534 C.C. Little Bldg, 1100 N. University, Ann Arbor, MI 48109-1005, USA

^d Korea Polar Research Institute, Songdo Techno Park 7-50, Songdo-dong, Yeonsu-gu, Incheon 406-840, South Korea

^e School of Earth and Environmental Sciences, Seoul National University, Seoul 151-747, South Korea

ARTICLE INFO

Article history:

Received 5 January 2010

Received in revised form 4 June 2010

Accepted 7 June 2010

Available online 8 July 2010

Editor: R.W. Carlson

Keywords:

Lu–Hf isotope

Re–Os isotope

Spitsbergen

peridotite

delamination

Paleoproterozoic/Neoproterozoic

ABSTRACT

The timing of sub-continental lithospheric mantle (SCLM) differentiation beneath Spitsbergen, western Svalbard, has been determined with spinel peridotite xenoliths using two complementary isotopic systems: Lu–Hf and Re–Os. The whole-rock Re–Os systematics (Re–Os errorchron, aluminochron, and Re-depletion age) define Paleoproterozoic/Neoproterozoic ages for isolation of the studied peridotites from the convecting mantle. We note that the age is independently supported by the Lu–Hf errorchron for the peridotite clinopyroxene grains, and average degree of melt depletion recorded in the samples. The obtained ages are indistinguishable from the oldest crustal ages reported in western Spitsbergen, implying that the mantle lithosphere in this area was stabilized at the same time as formation of the overlying crust. Our data suggest that the Spitsbergen lithosphere is unlikely to have undergone bulk lithospheric delamination since the tectonic transition from transpressional to transtensional which commenced in the Paleocene. We thus discount the delaminated and reactivated SCLM as a potential source for the Dupal-like enriched components in the Arctic upper mantle suggested by other studies.

© 2010 Elsevier B.V. All rights reserved.

1. Introduction

Determining the age of lithospheric mantle offers critical information about development and stabilization of the continents and the genetic relationship between the mantle lithosphere and overlying crust. It also provides insights into mantle dynamics such as the potential contribution of delaminated and foundering mantle lithosphere to the source of geochemically enriched mantle components in derivative basaltic magmas. The unique geochemical characteristics of the Re–Os parent–daughter system provide insights into the timing of melt depletion events (hence lithospheric mantle stabilization) in peridotites, because partial melting fractionates Re from Os owing to Re being moderately incompatible while Os is strongly compatible. As melting lowers the Re/Os ratio of the residue, the time-integrated Os isotopic composition of that material experiences minimal to no radiogenic growth unlike the convecting mantle below. Furthermore, because the Os concentration in peridotites is 10 to 1000 times greater than in the derivative silicate melts or other metasomatic agents, the Os isotopic system in peridotites is thought to be more resistant to secondary overprinting compared with other radiogenic isotope

systems (e.g., Sm–Nd and Rb–Sr) for which both parent and daughter elements behave incompatibly during mantle melting (e.g., Shirey and Walker, 1998).

Similarly, the Lu–Hf system has previously been shown to suffer no major effects from metasomatic processes and probably has a higher closure temperature than the Sm–Nd system, because (i) Hf has a considerably smaller diffusivity in silicate minerals than does Nd, and (ii) the relative difference in Hf concentration between melt and peridotites is lower than that in Nd concentration for the same materials (Pearson and Nowell, 2003; Choi et al., 2006, 2008; Bizimis et al., 2007; Wittig et al., 2007). Choi et al. (2008) demonstrated recently that the Lu–Hf system can be used to constrain the timing of lithospheric mantle differentiation and the study presented here supports that assertion.

Our study area, Svalbard Archipelago, is located on the north-westernmost edge of the Eurasian Plate, near the Knipovich Ridge and Gakkel Ridge in the North Atlantic and Arctic Oceans, respectively (Fig. 1A). Peridotite xenoliths brought to the surface by Quaternary volcanism on northwestern Spitsbergen, Svalbard, represent continental lithospheric mantle in the vicinity of oceanic spreading centers, and as such likely record the melt-extraction history and possibly even metasomatism in this tectonic setting. Previous work on these xenoliths mainly focused on the nature of metasomatism: processes, sources, and melt–fluid compositions (Amundsen, 1987; Ionov et al.,

* Corresponding author. Tel.: +82 42 821 6428; fax: +82 42 822 7661.

E-mail address: chois@cnu.ac.kr (S.H. Choi).

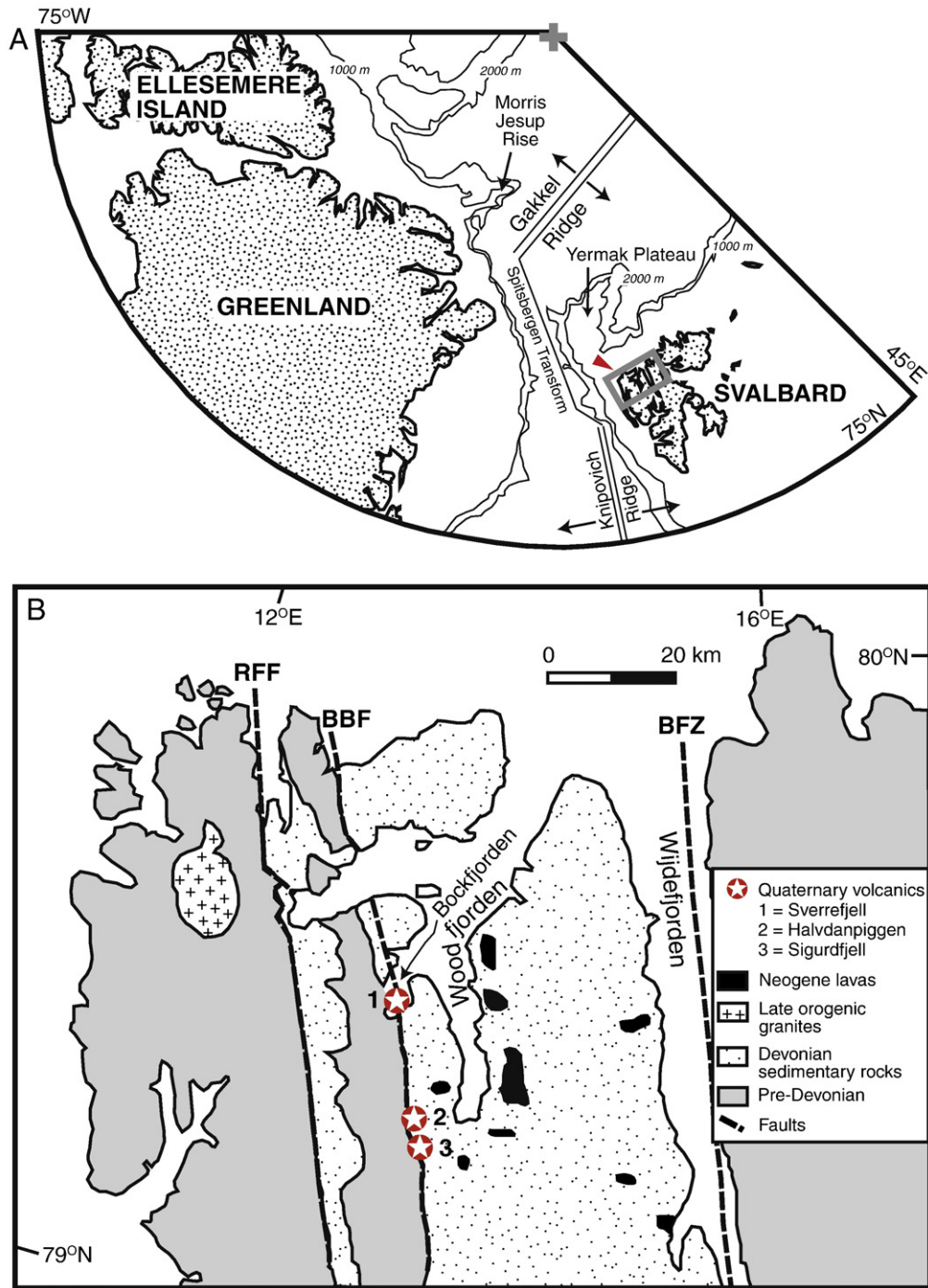


Fig. 1. (A) Location of Svalbard, and (B) simplified geological map of NW Spitsbergen (after Harland, 1997). Marine bathymetry is indicated by 1000 m and 2000 m contours in (A). BBF = Breibogen fault; BFZ = Billefjorden fault zone; RFF = Raudfjorden fault.

1993, 1996, 2002a,b). The work showed that (1) residual Spitsbergen peridotite protoliths were affected by carbonate-rich silicate melt percolation, and (2) the metasomatic source is not directly related to the source regions of the host basalts. Recently, Goldstein et al. (2008) argued that delaminated and dispersed Svalbard lithospheric mantle during continental break-up might have been the source for the Dupal-like isotopic signature observed in basalts along the western Gakkel Ridge. Jung et al. (2009) reported deformation microstructures and water content of olivine in the peridotite xenoliths of the study area. We present here the first ever Lu–Hf and Re–Os isotopic determinations for the peridotite xenoliths from Spitsbergen. Our aim is to constrain the age of lithospheric mantle stabilization beneath the

study area based on the two complementary systems, and to test the lithosphere delamination hypothesis.

2. Geological framework

Spitsbergen is the largest island in the Svalbard Archipelago of the Arctic Ocean, located midway between Norway and the North Pole (Fig. 1A). Tectonic reconstructions indicate that Svalbard was continuous with Greenland until the continental break-up and initiation of seafloor spreading between Norway and Greenland in the late Paleocene/early Eocene (Talwani and Eldhom, 1977; Johansson et al., 2005). The break-up of Laurasia along spreading

centers in the North Atlantic, Labrador Sea, and Eurasian Basin caused a transpressive tectonic regime on Svalbard during the Paleocene and Eocene, resulting in the creation of the Spitsbergen Transform Zone (Harland, 1969; Crane et al., 1982; Tuchschnid and Spillmann, 1992) (Fig. 1A). With cessation of sea floor spreading in the Labrador Sea in early Oligocene, the tectonic regime changed to transtensive, leading to oblique extension in the Spitsbergen Transform Zone (Lena Trough), and increased spreading along the Knipovich Ridge (Talwani and Eldhom, 1977; Hellebrand and Snow, 2003; Ljones et al., 2004). Sea floor spreading has propagated northward with time, resulting in linkage of the Arctic and North Atlantic at ca. 10 Ma (Eldholm et al., 1994; Blythe and Kleinspehn, 1998).

Two distinct phases of volcanism are known in Spitsbergen, the first consisting of Neogene lava flows, and the second, of Quaternary volcanic centers (Fig. 1B). Neogene lavas are largely subalkaline olivine tholeiitic basalts, whereas Quaternary volcanism has nepheline basanite/nepheline hawaiite rock composition. The volcanic centers are bound by N–S trending faults which project towards the Yermak Plateau and parallel the Spitsbergen Transform Zone (Fig. 1A, B). The faults are considered to have been established or reactivated during continental fragmentation (e.g., Amundsen et al., 1987; Skjeltkvåle et al., 1989). The volcanism is thus considered to be related to the opening of the eastern Arctic Basin and the Greenland Sea (Vogt et al., 1978; Feden et al., 1979), and the anomalously high heat flow on the Yermak Plateau, associated with reactivation of the Yermak hotspot (Crane et al., 1982; Tuchschnid and Spillmann, 1992).

Quaternary volcanic activity is found at three centers (Sverrefjell, Sigurdfjell and Halvdanpiggen) in the Bockfjorden area, NW Spitsbergen, along the trace of the Breibogen Fault zone (Fig. 1B). The fault trends NNW–SSE and juxtaposes Mesoproterozoic marbles and gneiss – overprinted by Caledonian deformation – to the west against Devonian sedimentary rocks in the east (Fig. 1B). The volcanic centers consist of basanite/hawaiite lava flows, pyroclastics and a hypabyssal intrusion. All centers contain abundant uppermost mantle and lower crustal xenoliths (Amundsen et al., 1987; Skjeltkvåle et al., 1989). Samples for this study were collected from Sverrefjell, the richest xenolith locality.

3. Samples and petrography

Samples selected for this study include spinel lherzolites and spinel harzburgites. Table 1 gives a summary of the petrography, Mg# (= $100\text{Mg}/(\text{Mg} + \text{Fe})$) of olivine, Cr# (= $100\text{Cr}/(\text{Cr} + \text{Al})$) of spinel, and estimates of equilibration temperatures for the mineral assemblages in these samples. Mg#s of olivine vary from 90.3 to 92.3, and Cr#s of spinel from 9.7 to 60.0. The modal mineralogy of the xenoliths has been determined from calculations using bulk rock chemistry and mineral compositions. Sample SVF-26 shows direct evidence of modal metasomatism, where amphibole occurs as large equigranular grains, suggesting textural equilibrium with coexisting silicates. This sample has been included to help evaluate the effects of metasomatism on the Lu–Hf systematics. A few samples containing carbonate-bearing pockets were also collected to cover the more extreme end of the compositional spectrum. The pockets (up to 500 μm in size) consist of carbonate aggregates, second generation clinopyroxene and olivine, silicate glass, and relict grains of resorbed minerals of the host peridotite, which are usually locate around spinel. Based on textural and geochemical data, previous studies (Ionov et al., 1996; Ionov, 1998) suggested that the Spitsbergen carbonate-bearing pockets were produced by reaction of carbonate-rich mantle melt with the host peridotites shortly before their transport to the surface as xenoliths. Sulfides are present in most of the xenoliths, both as isolated inclusions within silicate phases and as interstitial components (Table 1; Fig. S1). Trapped inclusions in silicates are rounded blebs. Interstitial grains occur along grain boundaries, or as a tiny bleb trails cross cutting the silicate grains. The size of individual sulfide grains is variable (up to 200 μm in diameter); larger grains are generally enclosed in the silicate phases. Lherzolites have higher modal contents of sulfides than the harzburgites. The major element compositions of representative sulfides are given in Supplementary Table 1. They are monosulfide solid solution (MSS), exsolved into Ni-rich MSS to pentlandite with minor chalcopyrite.

Equilibration temperatures were estimated by two-pyroxene thermometer of Wells (1977), and Al–Cr exchange thermometer of Witt-Eickschen and Seck (1991) based on the Al–Cr partitioning between orthopyroxene and spinel coexisting with olivine. The

Table 1
Sample list and information summary for Spitsbergen peridotite xenoliths studied.

Sample no	Rock type	Group	Texture	Modes					Accessory minerals	Microstructural position of sulfides	Equilibration temperature		Al ₂ O ₃ (wt.%)	Mg# in ol	Cr# in sp
				ol	opx	cpx	sp	amp			Two-pyroxene	Al–Cr opx			
				(wt.%)							(°C)				
SVF-04	sp.lz	c	proto	70.9	21.3	6.0	1.8	–	(sul)	e (opx)	972	949	1.94	91.9	20.0
SVF-05	sp.lz	b	proto	52.3	33.0	13.3	1.4	–	carb, sul	e (opx), i	998	978	2.66	90.9	16.9
SVF-09	sp.hz	c	proto-porphy	68.6	28.1	2.7	0.6	–	carb	i	993	954	0.85	91.4	42.7
SVF-26	sp.lz	c	proto	54.7	31.2	12.4	1.3	0.4	sul	i	1024	988	2.88	90.4	12.3
SVF-30	sp.lz	a	proto-porphy	62.3	26.7	8.7	2.3	–	carb, sul	e (opx), i	908	892	2.43	91.2	15.0
SVF-36	sp.hz	b	proto	76.1	21.6	1.8	0.5	–	carb, sul	i	894	914	0.75	91.7	20.9
SVF-41	sp.hz	c	porphy	81.8	16.1	1.2	0.9	–	(sul)	e (ol, opx), i	903	925	0.62	92.3	32.7
SVF-42	sp.hz	c	proto	61.4	37.5	0.2	0.9	–					0.51	92.3	60.0
SVF-47	sp.lz	b	porphy	48.1	37.3	12.6	2.0	–	(sul)	i	840	903	2.89	90.8	12.9
SVF-48	sp.lz	b	porphy	48.8	40.1	9.3	1.8	–	sul	e (opx), i	856	880	2.69	90.9	11.8
SVF-49	sp.lz	a	porphy	53.8	35.1	9.5	1.6	–	sul	i	895	890	2.06	91.1	17.9
SVF-50	sp.lz	a	porphy	51.3	35.9	10.8	2.0	–	sul	i	882	888	3.02	90.3	10.6
SVF-51	sp.lz	b	porphy	56.4	36.3	6.5	0.8	–	sul	e (opx), i	880	901	1.27	91.8	28.2
SVF-52	sp.hz	b	porphy	62.8	34.1	2.5	0.6	–	sul	e (ol, opx), i	850	908	1.34	91.1	17.4
SVF-53	sp.lz	a	porphy	56.8	31.3	10.7	1.2	–	sul	i	925	902	2.06	91.1	16.4
SVF-61	sp.lz	a	porphy	49.3	38.4	10.4	2.0	–	sul	e (ol, cpx), i	858	855	2.95	90.5	9.7

Sample location: 12°21'50"E, 79°26'50"N.

Equilibration temperatures were estimated by two-pyroxene thermometer of Wells (1977), and Al–Cr exchange thermometer of Witt-Eickschen and Seck (1991).

Modal compositions were calculated from whole-rock and mineral compositions by least-squares method.

Abbreviations: sp.lz = spinel lherzolite; sp.hz = spinel harzburgite; proto = protogranular; porphy = porphyroclastic; ol = olivine; opx = orthopyroxene; cpx = clinopyroxene; Sp = spinel; amp = amphibole; carb = carbonate-bearing pocket; sul = sulfide; e = enclosed in silicate grains; i = interstitial.

Mg# = $100\text{Mg}/(\text{Mg} + \Sigma\text{Fe})$.

Cr# = $100\text{Cr}/(\text{Cr} + \text{Al})$.

equilibration temperatures range from 840 to 1020 °C (Table 1), which is within the range of temperatures (840 to 1170 °C) reported for Spitsbergen peridotites by Amundsen et al. (1987) and Ionov et al. (2002a). Amundsen et al. (1987) constructed a geotherm for northwestern Spitsbergen based on equilibrium *P*–*T* estimates for garnet websterite xenoliths, and temperature estimates for two-pyroxene granulite and spinel lherzolite xenoliths. Projection of the temperature estimates for the samples studied onto the Spitsbergen geotherm yields pressures of 7 to 11 kbar.

4. Analytical methods

The xenoliths range in size from 6 to 13 cm in their longest dimension. Samples for whole-rock analysis were prepared from the core of each xenolith, free of any visible surface weathering. The rock samples were first coarsely crushed to expose interior fragments of the xenoliths using a tungsten-carbide pestle wrapped in paper to avoid contamination. They were then disaggregated using first an agate mortar and pestle followed by grinding into a fine powder with an alumina ball mill. This produced 20 to 30 g of powder for each sample. Clinopyroxene is the major carrier of REE and possibly Hf in the anhydrous spinel peridotite mineral assemblages (e.g., Eggins et al., 1998; Bedini and Bodinier, 1999; Choi et al., 2008). To avoid the effects of infiltration by the magmas that carried the xenoliths to the surface or alteration by a near-surface fluid, we limited our Nd and Lu–Hf isotopic analyses to ultra-pure clinopyroxene separates. We treat the data for this mineral as representative of each xenolith. Clinopyroxene grains were prepared from unweathered, disaggregated sample fragments using nylon sieves for sizing, a magnetic separator to eliminate grains with dark inclusions, and hand picking under a binocular microscope to select only the optically clear grains for analysis. Prior to dissolution for the isotopic analyses, the minerals were washed in warm, distilled 2.5 N HCl for 15 min, and in warm distilled 5% HF for 15 min, with an H₂O rinse after each of these steps.

Major-element concentrations have been determined by X-ray fluorescence (XRF) spectrometry on fused disks at Act Labs in Ontario, Canada (Supplementary Table 2). Rare-earth-element concentrations in clinopyroxene have been measured by inductively-coupled-plasma mass spectrometry (ICP-MS) at the Korea Polar Research Institute. Standards (JGB-1 and JR-1) have been analyzed with the unknown samples, and their values are reported in Supplementary Table 3. Samples were dissolved in a mixture of

ultra-pure, concentrated HF–HNO₃–HClO₄. Precision was estimated to be within 10%.

Nd and Lu–Hf isotope analyses, including chemical separation and measurements, were performed at the University of Michigan. Details of the analytical procedures appear in Choi et al. (2008). The Nd isotope analyses were performed with VG Sector thermal ionization mass spectrometers. ¹⁴³Nd/¹⁴⁴Nd ratios were corrected for instrumental mass fractionation by normalizing to ¹⁴⁶Nd/¹⁴⁴Nd = 0.7219. Replicate analyses of La Jolla standards gave ¹⁴³Nd/¹⁴⁴Nd = 0.511850 ± 19 (*N* = 30, 2σ). The Hf isotope analyses were determined with the multiple-collector ICP-MS (Nu-Plasma HR). Lu and Hf concentrations were measured by isotope dilution with enriched ¹⁷⁶Lu and ¹⁷⁸Hf spikes. In order to monitor machine performance, the JMC-475 standard was run after every three samples obtaining a mean ¹⁷⁶Hf/¹⁷⁷Hf ratio of 0.282150 ± 12 (*N* = 10, 2σ), and the values reported were normalized to the accepted value of 0.282160. Total blanks averaged 0.04 ng for Nd, and 0.02 ng for Hf. The results are given in Table 2.

Re–Os isotope analyses, including chemical separation and measurements, were performed at Japan Agency for Marine–Earth Science and Technology (JAMSTEC). Details of the analytical procedures appear in Suzuki et al. (2004) and Kato et al. (2005). Briefly, approximately ~0.5 g of pulverized whole-rock sample aliquots with ¹⁸⁵Re and ¹⁹⁰Os spikes were dissolved in Carius tube. This was followed by Os extraction with carbon tetrachloride and its purification by microdistillation. Re purification was carried out on anion exchange columns using AG 1 × 8 resin (100–200 mesh). Re and Os were loaded onto Pt filaments with Ba(NO₃)₂ as an activator. The Re–Os isotope analyses were determined with a ThermoFinnigan TRITON®, in negative ion detection mode. Total blank levels were ~7.0 pg for Re and ~2.2 pg for Os with ¹⁸⁷Os/¹⁸⁸Os of ~0.17. Contribution of the blank to measured Os concentrations and ¹⁸⁷Os/¹⁸⁸Os were <0.1%. Precision of ¹⁸⁷Re/¹⁸⁵Re and ¹⁸⁷Os/¹⁸⁸Os measurements, based on analysis of an in-house standard over a period of several months, was better than 0.1% (1σ) and 0.3% (1σ), respectively. The results are given in Table 3.

Reproducibility based on replicate analyses of a high-concentration Os sample (SVF-41) was calculated to be 18% for Os concentrations, and 0.8% for the ¹⁸⁷Os/¹⁸⁸Os values. This is typical of platinum group element (PGE) data in general (e.g., Handler and Bennett, 1999; Alard et al., 2005). These variations can be attributed to the so-called nugget effect, which refers to heterogeneous distribution of PGE-bearing trace phases in a sample.

Table 2
Lu–Hf and Nd isotopic compositions for clinopyroxenes from Spitsbergen peridotite xenoliths, and for the host basanite.

Sample no	Rock type	Lu (ppm)	Hf (ppm)	¹⁷⁶ Lu/ ¹⁷⁷ Hf	¹⁷⁶ Hf/ ¹⁷⁷ Hf	2σ	ε _{Hf}	¹⁴³ Nd/ ¹⁴⁴ Nd	2σ	ε _{Nd}
SVF-05	sp.lz	0.19	0.46	0.0591	0.284655	28	66.6	0.513075	22	8.5
SVF-09	sp.hz	0.12	0.36	0.0464	0.283779	30	35.6	0.512916	21	5.4
SVF-26	sp.lz	0.23	0.78	0.0426	0.283674	10	31.9	0.512693	20	1.1
SVF-30	sp.lz	0.27	1.11	0.0350	0.283724	13	33.7	n.d.	n.d.	n.d.
SVF-42	sp.hz	0.06	0.19	0.0484	0.284561	42	63.3	0.512949	19	6.1
SVF-47	sp.lz	0.24	0.95	0.0363	0.283442	16	23.7	n.d.	n.d.	n.d.
SVF-48	sp.lz	0.26	0.85	0.0435	0.283839	9	37.7	0.513176	25	10.5
SVF-49	sp.lz	0.20	0.17	0.1569	0.286988	38	149.1	0.513087	16	8.8
duplicate		0.20	0.17	0.1596	0.286993	57	149.3	n.d.	n.d.	n.d.
triplicate					0.286897	166	145.9	n.d.	n.d.	n.d.
SVF-50	sp.lz	0.29	0.89	0.0467	0.284463	10	59.8	0.513453	15	15.9
SVF-52	sp.hz	0.22	0.97	0.0318	0.283388	18	21.8	0.513003	18	7.1
SVF-53	sp.lz	0.21	0.48	0.0635	0.284083	18	46.4	0.513177	17	10.5
SVF-61	sp.lz	0.30	1.05	0.0409	0.283765	20	35.1	0.513334	17	13.6
SVF H-2	basanite	0.17	5.35	0.0045	0.283245	4	16.7	0.512916	17	5.4

ε_{Hf} and ε_{Nd} are calculated with ¹⁷⁶Hf/¹⁷⁷Hf = 0.282772 and ¹⁴³Nd/¹⁴⁴Nd = 0.512638 for present-day chondritic Earth.

sp.lz = spinel lherzolite; sp.hz = spinel harzburgite.

n.d. = not determined.

Table 3
Re–Os isotopic compositions for Spitsbergen whole-rock peridotite xenoliths.

Sample no	Rock type	Re (ppt)	Os (ppt)	$^{187}\text{Re}/^{188}\text{Os}$	$^{187}\text{Os}/^{188}\text{Os}$	2σ	T_{RD} (Ga)	T_{MA} (Ga)	γ_{Os}
SVF-04	sp.lz	28	2640	0.051	0.1166	2	1.78	2.0	−10.0
SVF-36	sp.hz	170	4227	0.194	0.1131	1	2.24	4.0	−12.7
SVF-41	sp.hz	30	6134	0.024	0.1096	4	2.71	2.9	−15.4
duplicate		34	5025	0.032	0.1087	1	2.83	3.1	−16.1
SVF-48	sp.lz	221	3727	0.285	0.1207	1	1.22	3.5	−6.9
SVF-49	sp.lz	194	4439	0.211	0.1223	1	1.00	1.9	−5.6
SVF-50	sp.lz	150	3437	0.210	0.1256	2	0.55	1.1	−3.1
SVF-51	sp.lz	56	4322	0.063	0.1192	2	1.42	1.7	−8.0
SVF-52	sp.hz	85	1990	0.206	0.1207	3	1.22	2.3	−6.9
SVF-53	sp.lz	109	3410	0.154	0.1208	5	1.21	1.9	−6.8
SVF-61	sp.lz	100	3562	0.135	0.1215	2	1.11	1.6	−6.3

All data are blank-corrected.

The $^{187}\text{Os}/^{188}\text{Os}$ ratios are less than the 2-sigma reproducibility (0.6%) in the measurements of our Os standard.

Values of primitive upper mantle ($^{187}\text{Re}/^{188}\text{Os}=0.433$ and $^{187}\text{Os}/^{188}\text{Os}=0.1296$; Meisel et al., 2001) are used for the calculation of T_{RD} and T_{MA} ages, and γ_{Os} .

sp.lz = spinel lherzolite; sp.hz = spinel harzburgite.

5. Results

5.1. Whole-rock chemistry

The whole-rock Mg# values of the Spitsbergen peridotites studied range from 89.5 to 91.9 (Supplementary Table 2). Variations in representative major oxides (Al_2O_3 and CaO) as a function of MgO, good indicators of degree of depletion of the peridotites, are shown in Fig. 2A–B. Available data from previous study are shown for comparison. Spitsbergen peridotites are characterized by a wide range of compositional variation, extending from mildly depleted lherzolites (Al_2O_3 up to 3 wt.%), through harzburgites similar to typical abyssal peridotites, into the field of Archean cratonic harzburgites from East Greenland (Bernstein et al., 1998; Hanghøj et al., 2001) (Fig. 2A–B). The abundance and trends are compatible with the best-fit lines for world-wide spinel peridotite xenolith compositions, suggesting that the rocks are for the most part residues after variable degrees of basaltic melt extraction. We note that the samples containing carbonate-bearing pockets are not offset on the MgO vs. CaO plot, suggesting that the modal abundance of carbonates is not significant. The samples also do not display any significant FeO enrichment (Supplementary Table 2), even in the amphibole-bearing peridotite, ruling out amphibole formation from an evolved Fe-rich basaltic melt.

5.2. Rare earth element chemistry

Rare earth elements (REE) concentrations for the clinopyroxenes from the Spitsbergen peridotites are listed in Supplementary Table 3. Chondrite-normalized REE patterns are shown in Fig. 3. The heavy rare earth elements (HREE), such as Lu, which are moderately incompatible in clinopyroxene have abundances which correlate positively with indices of melt depletion (e.g., Al_2O_3) (Supplementary Tables 2 and 3; Fig. 4A), supporting an origin for the peridotites as residues after variable degrees of melt depletion. Meanwhile, the REE patterns for the clinopyroxene grains are variable from light rare earth element (LREE) depleted through spoon-shaped to LREE-enriched (Fig. 3A–C). These characteristics are not consistent with simple melt extraction, but instead reflect some overprinting by secondary metasomatism in the history of the xenoliths, as discussed in previous studies of the Spitsbergen peridotites (Ionov et al., 2002a,b). In order to evaluate the effect of metasomatism, we divide the samples into three groups. Group *a* samples (SVF-30, -49, -50, -53 and -61) retain residual characteristics inasmuch as they show LREE-depleted patterns and exhibit only very slight incompatible trace element enrichments. The degree of metasomatic overprinting thus increases

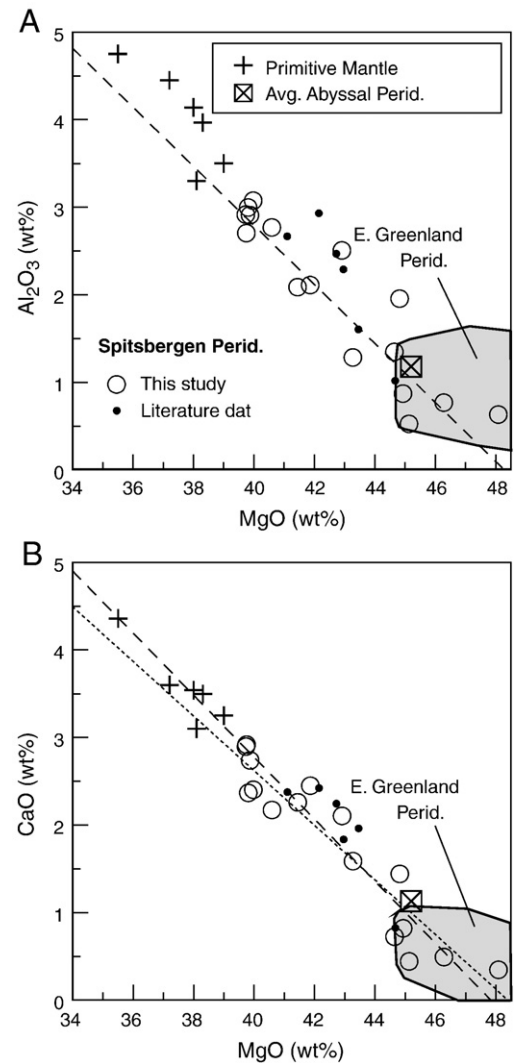


Fig. 2. Major oxide compositional variations for the Spitsbergen peridotites. The dashed lines are the best-fit lines for spinel lherzolite xenoliths from other localities in Maaløe and Aoki (1977), and the dotted line from McDonough (1990). Literature data for the Spitsbergen peridotites are from Ionov et al. (2002a). Data sources: primitive mantle (Palme and Nickel, 1985; McDonough, 1990 and references therein), average abyssal peridotite (Boyd, 1989), East Greenland peridotites (Bernstein et al., 1998).

from group *a* toward group *b* (SVF-5, -36, -47, -48, -51 and -52) to *c* (SVF-4, -9, -26, -41 and -42). Chondrite-normalized $(\text{Ce}/\text{Yb})_{\text{N}}$ ratios vary from 0.3 to 1.3 for group *a*, 2.2 to 3.3 for group *b* (except SVF-51), and 3.9 to 20.5 for group *c* (Supplementary Table 3). Sample SVF-49 displays a fractionated HREE pattern, indicating that garnet might have been involved in the source.

5.3. Nd and Lu–Hf isotopes

The Nd and Lu–Hf isotopic compositions were obtained for clinopyroxene separates from 12 peridotites and the host basanite (Table 2). The Nd, Lu and Hf concentrations of clinopyroxene grains from Spitsbergen peridotites vary from 2.0 to 24.4 ppm, from 0.1 to 0.4 ppm, and from 0.2 to 1.1 ppm, respectively (Table 2; Supplementary Table 3; Fig. 4A–C), which lie within the range measured for other spinel peridotite xenoliths (e.g., Bizimis et al., 2003; Carlson et al., 2004; Choi et al., 2008). The clinopyroxene grains display a wide range in Nd isotopic compositions ($^{143}\text{Nd}/^{144}\text{Nd}=0.512693$ to 0.513453 ; $\epsilon_{\text{Nd}}=+1.1$ to $+15.9$), and an extremely wide range in Hf isotopic compositions ($^{176}\text{Hf}/^{177}\text{Hf}=0.283388$ to 0.286993 ; $\epsilon_{\text{Hf}}=+21.8$ to $+149.3$) and elemental ratios ($^{176}\text{Lu}/^{177}\text{Hf}=0.03$ to 0.19). Host basanite has $^{143}\text{Nd}/^{144}\text{Nd}=\text{---}$

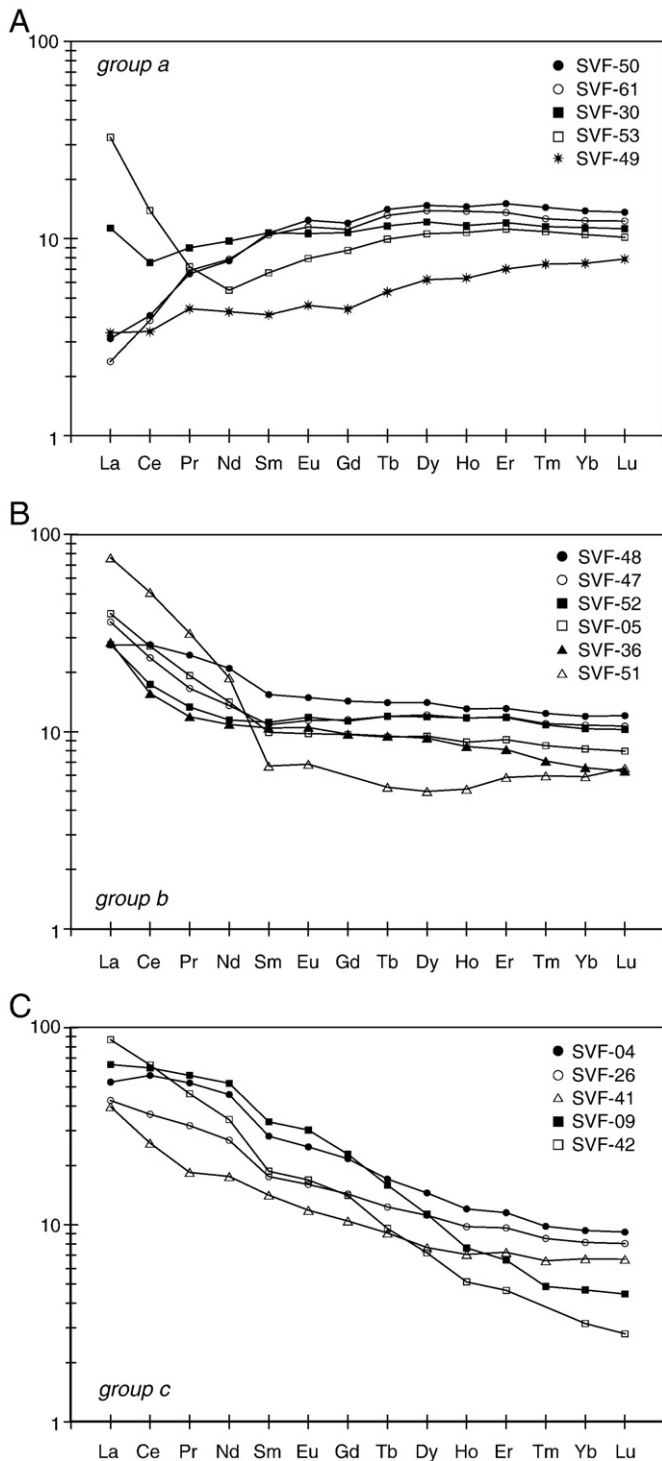


Fig. 3. Rare-earth element abundances for clinopyroxene from the Spitsbergen peridotites, normalized to the chondritic values in Sun and McDonough (1989).

0.512916 ($\epsilon_{\text{Nd}} = +5.4$), and $^{176}\text{Hf}/^{177}\text{Hf} = 0.283245$ ($\epsilon_{\text{Hf}} = +16.7$). Our result on the Nd isotopic composition of host lava is in good agreement with the earlier data by Ionov et al. (2002b). The Nd–Hf isotopic correlation diagram is shown in Fig. 5A. For comparison, the fields for MORB (mid-ocean ridge basalts) and OIB (oceanic island basalts), and the Nd–Hf ‘mantle array’ are also shown on the diagram. Two general observations are patently obvious: (1) the Nd and Hf isotopic compositions of all Spitsbergen samples are depleted relative to the bulk silicate earth value (Fig. 5A); and (2) Spitsbergen peridotite clinopyroxenes are

characterized by strong Nd–Hf decoupling compared to the mantle array, whereas the host basaltic plots within the field of oceanic basalts which define the array (Fig. 5A). It is remarkable that sample SVF-49 exhibits strongly depleted Hf isotopic composition ($\epsilon_{\text{Hf}} = +149$), in marked contrast to the present-day oceanic basalt mantle source. To test for reproducibility, we ran the sample in triplicate. The extreme Hf isotopic composition was reproduced within uncertainty (Table 2). Fig. S2 and Fig. 5B are the Sm–Nd and Lu–Hf isochron diagrams for the clinopyroxene separates from the xenoliths, respectively. Also plotted in the diagrams are available present-day DM (depleted mantle) values for reference, and Sm–Nd isotopic compositions for Spitsbergen peridotites (Ionov et al., 2002b). Group a samples have higher $^{147}\text{Sm}/^{144}\text{Nd}$ and $^{143}\text{Nd}/^{144}\text{Nd}$ ratios than the DM, in contrast to the group b and c samples which have lower values (Fig. S2). Meanwhile, all but two samples have higher $^{176}\text{Lu}/^{177}\text{Hf}$ and $^{176}\text{Hf}/^{177}\text{Hf}$ ratios compared with DM (Fig. 5B). Sample SVF-49 has a highly elevated $^{176}\text{Lu}/^{177}\text{Hf}$ ratio, compared with the other samples (Fig. 5B). Therefore, the extremely depleted Hf isotopic composition reflects a time-integrated record of radiogenic Hf ingrowth associated with this high Lu/Hf. The elevated Lu/Hf ratio indicates that these clinopyroxene grains are likely to be the result of sub-solidus breakdown of garnet, which is consistent with the fractionated HREE pattern (Fig. 3A).

5.4. Re–Os isotopes

The Re–Os isotopic compositions were measured for ten whole-rock peridotites (Table 3). The Os concentrations of the Spitsbergen peridotites vary from 2.0 to 6.1 ppb, falling within the range for orogenic peridotites (global mean = 4.0 ± 1.6 ppb) and cratonic peridotite xenoliths (4.2 ± 2.7 ppb), but relatively higher than off-cratonic peridotite xenoliths hosted by alkali basalts (2.0 ± 1.1 ppb) (Pearson et al., 2004) (Table 3). The Re concentrations vary from 0.03 to 0.22 ppb, which is less than the primitive mantle value of 0.28 ± 0.08 ppb (McDonough and Sun, 1995) (Fig. 4d). This observation is consistent with variable Re loss through melt depletion. The xenoliths yield $^{187}\text{Os}/^{188}\text{Os}$ between 0.1087 and 0.1256, and $^{187}\text{Re}/^{188}\text{Os}$ ranging from 0.024 to 0.285. The Spitsbergen samples have lower $^{187}\text{Re}/^{188}\text{Os}$ and $^{187}\text{Os}/^{188}\text{Os}$ ratios ($\gamma_{\text{Os}} = -16$ to -3) than the estimates for the primitive upper mantle (PUM) (Meisel et al., 2001) (Fig. 6A, B), reflecting long-term isolation in a low Re/Os environment produced by ancient partial melting. Conventional Re–Os model ages (T_{MA} ; Walker et al., 1989) – age of melt extraction occurred for individual peridotites from the intersection of two isotopic evolution paths defined by the present-day $^{187}\text{Os}/^{188}\text{Os}$ and $^{187}\text{Re}/^{188}\text{Os}$ ratios of the sample and PUM – range from 1.1 to 4.0 Ga with most falling within range of 1.6 to 2.0 Ga (Table 3). If the average chondritic mantle evolution curve ($^{187}\text{Re}/^{188}\text{Os} = 0.40186$, $^{187}\text{Os}/^{188}\text{Os} = 0.1270$; Shirey and Walker, 1998) is used instead for the calculation, the estimated ages decrease by ca. 0.3 Ga. There appears to be no visible relation between the model ages and microstructural positions of the sulfides observed in thin section, classified as interstitial or enclosed (Tables 1 and 3; Supplementary Table 1; Fig. S1). Recent studies indicate that silicate-enclosed sulfides may represent residues of partial melting processes, but interstitial sulfides are often considered to be crystallization products of sulfur-bearing fluids (Alard et al., 2000; Pearson et al., 2002). These earlier studies report differences in major element compositions according to microstructural positions of the sulfides, such as relatively Cu–Ni enrichment in interstitial sulfides compared to silicate-enclosed ones. By contrast, no significant chemical difference is observed among these different types of sulfides in the Spitsbergen peridotites. Interstitial sulfides in Spitsbergen peridotites may not have formed by new growth but by recrystallization. In Fig. 6A, we have compared our data with published whole-rock abyssal peridotite Os isotopic compositions, noting that the $^{187}\text{Os}/^{188}\text{Os}$ ratio of sample SVF-41 falls well below any estimates for abyssal peridotites, reinforcing it as a representative of ancient residues of partial melting.

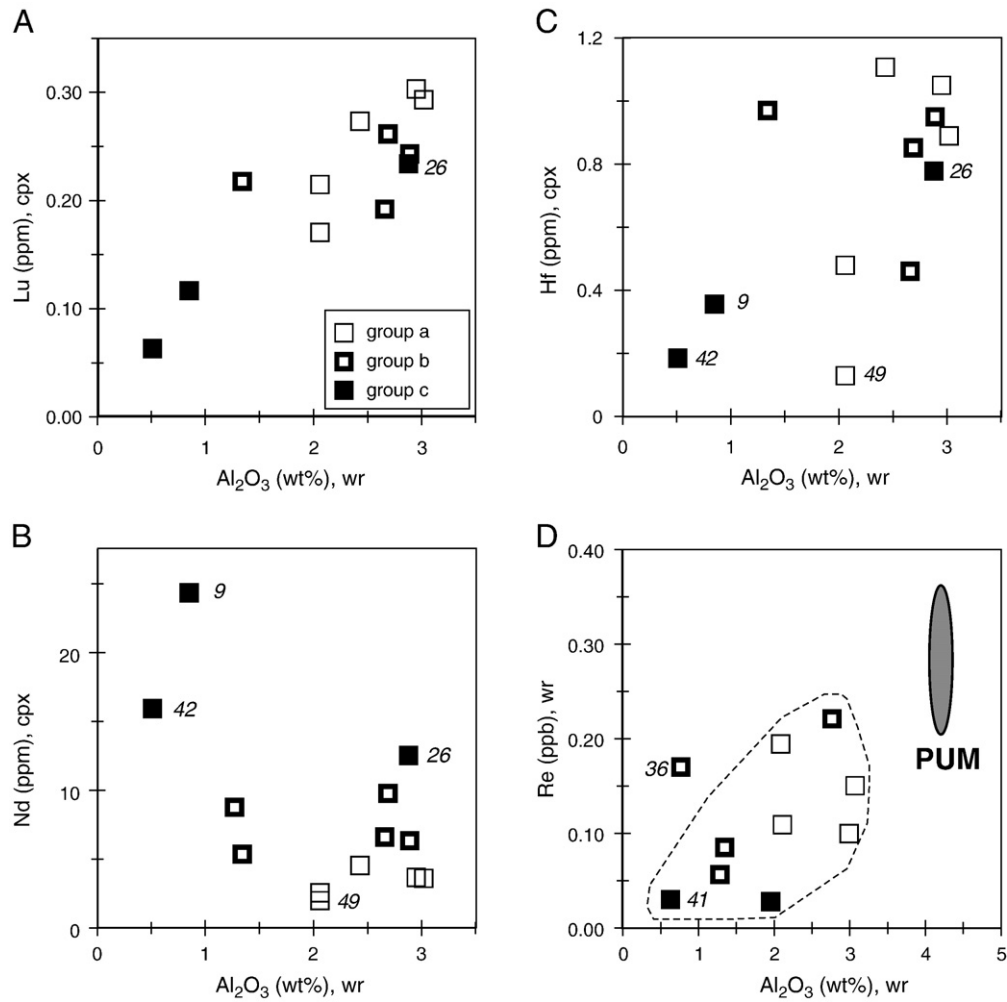


Fig. 4. (A) Lu, (B) Nd, and (C) Hf in clinopyroxene grains from Spitsbergen peridotites, (D) whole-rock Re vs. whole-rock Al_2O_3 concentrations. Primitive upper mantle (PUM) composition from McDonough and Sun (1995), and Meisel et al. (2001).

6. Discussion

6.1. Lu–Hf isotopic systematics

Previous studies (Ionov et al., 1996; 2002a,b) considered the possibility that carbonate-rich silicate melts percolating through residual peridotites might have produced the Spitsbergen peridotites which show ample evidence for modal and/or cryptic metasomatism. In order to test the hypothesis that Nd and Hf might be mobile during metasomatic overprinting, we have plotted the Nd and Hf abundances and isotopic compositions of clinopyroxenes from the Spitsbergen peridotites as a function of whole-rock Al_2O_3 concentration (Fig. 4B, C; Fig. S3A, B). The Nd abundances display a rough negative correlation with Al_2O_3 (Fig. 4B), and increase from group *a* through group *b* to *c*. Group *a* is composed of relatively fertile lherzolites, while group *c* is dominated by harzburgites. Therefore, this apparently contradictory pattern of stronger LREE enrichment in the most depleted samples can be attributed to metasomatic enrichment in LREEs of residual rocks formed by earlier partial melting events, which is very common feature observed in peridotite suites (e.g., Frey and Green, 1974). Group *b* and *c* samples have lower values of $^{147}\text{Sm}/^{144}\text{Nd}$ and $^{143}\text{Nd}/^{144}\text{Nd}$ than those of the DM in Fig. S2 further supports this notion. Meanwhile, the Hf concentrations show a general positive trend with Al_2O_3 . We note that the two group *c* samples (SVF-9 and -42), which have the lowest Al_2O_3 but the highest Nd concentrations, do not display coherent enrichment in Hf with Nd (Fig. 4B, C). Furthermore, the Hf concentration of a

clinopyroxene from an amphibole-bearing peridotite (SVF-26) plots along the residual trend defined by the other samples (Fig. 4C). In addition, the clinopyroxene grains have a wide range in Nd isotopic compositions ($\epsilon_{\text{Nd}} = +1.1$ to $+15.9$) with a systematic decrease from group *a* through group *b* to *c*. The Nd isotopic compositions display a good positive trend with Al_2O_3 (Fig. S3A). This strongly contrasts with the Hf isotopic compositions which show an extremely wide range in ϵ_{Hf} ($+21.8$ to $+149.3$) without any systematic trend within the groups (Fig. 5A). In addition, most of the samples have elevated $^{176}\text{Lu}/^{177}\text{Hf}$ and $^{176}\text{Hf}/^{177}\text{Hf}$ ratios compared with the DM (Fig. 5B). These observations suggest that the Hf is much less susceptible to secondary overprinting by the carbonate-rich metasomatic melts than Nd. Therefore, we interpret the significant Nd–Hf isotopic decoupling observed in Fig. 5A to be the result of secondary metasomatism severely impacting the Sm–Nd system, but not the relatively more robust Lu–Hf system. Bizimis et al. (2003) showed that recent metasomatism of an ancient depleted peridotite through melt–rock reaction can generate Nd–Hf decoupling, similar to that seen in the Spitsbergen peridotites.

The $^{176}\text{Hf}/^{177}\text{Hf}$ ratios of lherzolites display a negative correlation with Al_2O_3 (Fig. S3B), supporting the notion that the Hf is immobile relative to Nd. Meanwhile, the Hf isotopic compositions of harzburgites (SVF-9, -42 and -52) plot outside the trend defined by lherzolites. It has been argued that orthopyroxene might be a significant repository for the HFSE (high-field-strength element) budget in anhydrous spinel peridotite (Rampone et al., 1991; Egginis et al., 1998; Bedini and Bodinier, 1999; Witt-Eickschen and O'Neill,

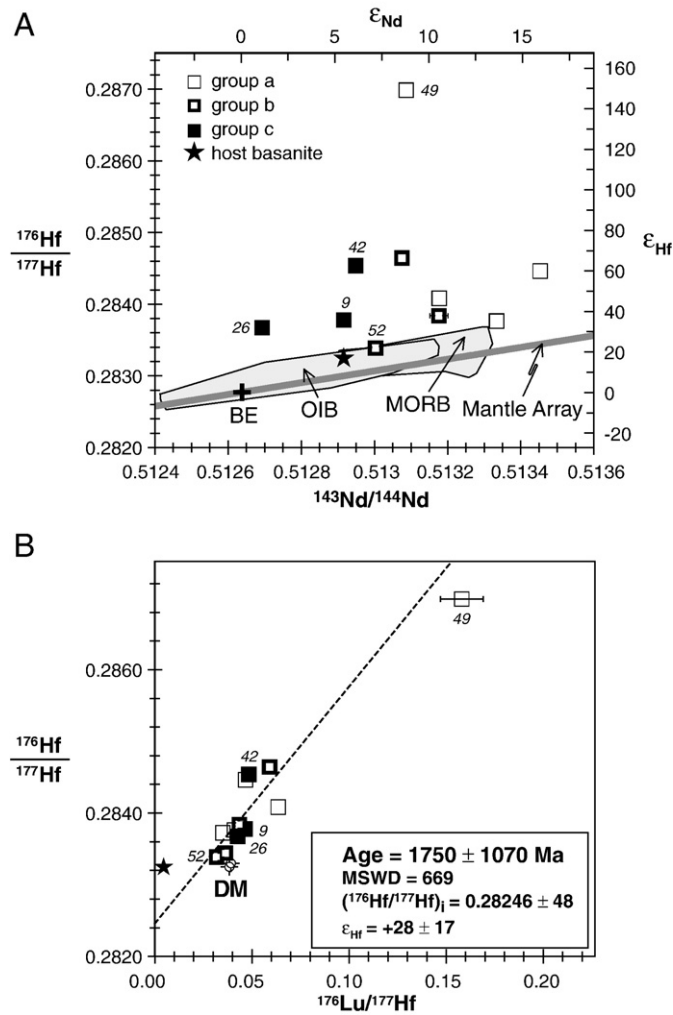


Fig. 5. (A) $^{176}\text{Hf}/^{177}\text{Hf}$ vs. $^{143}\text{Nd}/^{144}\text{Nd}$, and (B) $^{176}\text{Hf}/^{177}\text{Hf}$ vs. $^{176}\text{Lu}/^{177}\text{Hf}$ ratios for clinopyroxene separated from some Spitsbergen peridotites. All error bars are 2σ uncertainties, and are given only where they exceed the size of the symbol in the plot. Fields for oceanic basalts are from Salters (1996), Salters and White (1998), Chauvel and Blichert-Toft (2001), Andres et al. (2004), Hanan et al. (2004), and Blichert-Toft et al. (2005). The bulk Earth $^{176}\text{Hf}/^{177}\text{Hf}$ value (BE) and the Mantle array in (A) are from Blichert-Toft and Albarède (1997) and Blichert-Toft et al. (1999). The DM (depleted mantle) $^{176}\text{Lu}/^{177}\text{Hf}$ and $^{176}\text{Hf}/^{177}\text{Hf}$ values in (B) are from Nowell et al. (1998), Vervoort and Blichert-Toft (1999), and Griffin et al. (2000). The broken line in (B) is an errorchron for the samples studied. Calculation of the Lu–Hf errorchron is based on the decay constant $\lambda^{176}\text{Lu} = 1.865 \times 10^{-11} \text{ yr}^{-1}$ (Scherer et al., 2001). Sample SVF-49 is eliminated from the regression. MORB = mid-ocean ridge basalt; OIB = oceanic island basalt.

2005). When we consider the partitioning value of Hf between clinopyroxene and orthopyroxene, $D_{\text{Hf}}^{\text{cpx/ox}} \approx 25$ in anhydrous spinel peridotite at ca. 900 °C (Egginis et al., 1998; Bedini and Bodinier, 1999; Witt-Eickchen and O'Neill, 2005), the contribution of orthopyroxene to the whole-rock budget for Hf in Spitsbergen lherzolites is estimated to be only up to ~15%. Considering that the value of $D_{\text{Hf}}^{\text{cpx/amp}} \approx 1$ (Ionov et al., 2002a), then amphibole accounts for only 3% of the Hf in hydrous peridotite sample SVF-26. It appears that orthopyroxene and amphibole play only minor roles in the whole-rock Hf budget for the lherzolites. In harzburgites on the other hand, orthopyroxene can be a major repository of Hf. The high modal orthopyroxene/clinopyroxene ratio in Spitsbergen harzburgites results in the contribution of orthopyroxene ranging from 30 to 90% of the whole-rock Hf budget. Therefore, the offset observed in the correlation between Hf isotopic composition and whole-rock Al_2O_3 concentration (Fig. S3B) can be attributed to orthopyroxene control of the Hf budget in harzburgites.

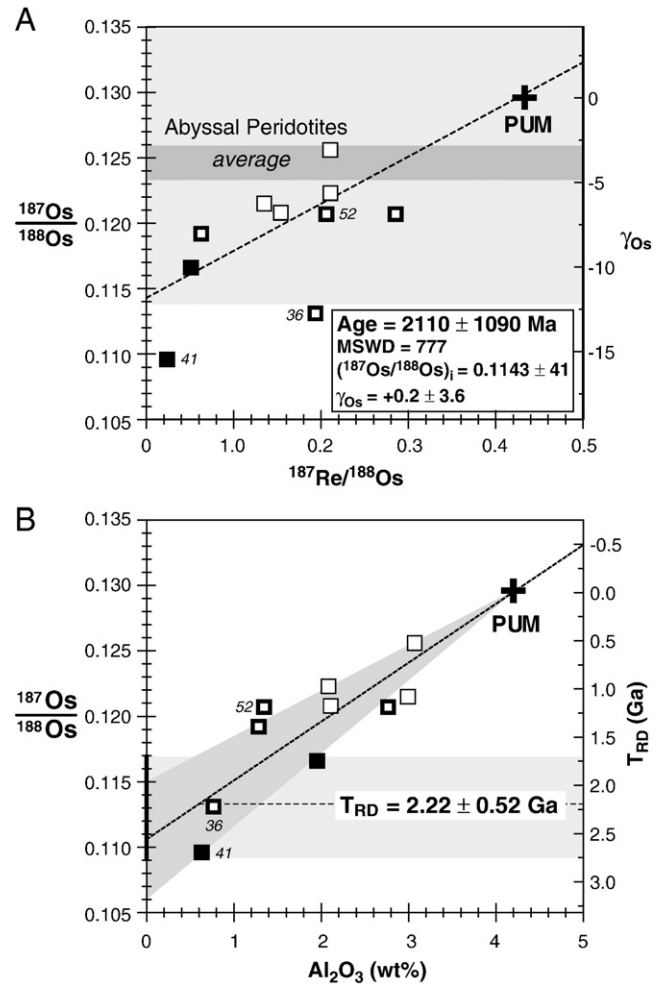


Fig. 6. (A) Re–Os isochron diagram for Spitsbergen peridotites. The shaded field represents the range of published $^{187}\text{Os}/^{188}\text{Os}$ values for whole-rock abyssal peridotites (Harvey et al., 2006 and references therein; Liu et al., 2008), with the proposed range of average abyssal peridotite at 0.1246 ± 14 (Snow and Reisberg, 1995). The broken line in (A) is an errorchron for the samples when it is forced through the hypothetical primitive upper mantle (PUM) composition of 0.1296 ± 8 (Meisel et al., 2001). Sample SVF-36 has been eliminated from the regression (see text). (B) $^{187}\text{Os}/^{188}\text{Os}$ vs. Al_2O_3 concentration (whole-rock). The broken line in (B) is a regression line for the samples ($R^2 = 0.78$). The $^{187}\text{Os}/^{188}\text{Os}$ ratio at $\text{Al}_2\text{O}_3 = 0.6 \text{ wt.}\%$ of the regression is used to determine the model age for formation of mantle lithosphere beneath Spitsbergen. All errors (2σ) are within the size of the symbol in the plot. Symbols as in Fig. 5.

The Spitsbergen peridotite clinopyroxenes define a positive correlation on a Lu–Hf isochron diagram (Fig. 5B). The samples yield an ‘errorchron’ age of $1.8 \pm 1.1 \text{ Ga}$ (2σ), an initial ϵ_{Hf} of $+28 \pm 17$ and a MSWD of 669 when the $\lambda^{176}\text{Lu}$ value of $1.865 \times 10^{-11} \text{ yr}^{-1}$ (Scherer et al., 2001) is used in the calculation. We interpret this Paleoproterozoic age to mark the time of stabilization of the mantle section by melt extraction, which will be supported by the Re–Os systematics in the next section below. Dating melting extraction by the Lu–Hf isochron method will be meaningful only if the original peridotites underwent melt extraction from an isotopically homogenous mantle source at the same time (or series of melting events closely spaced in time), and no Lu and Hf mobility has occurred since melt extraction. The large uncertainty might be due to a partial resetting by subsequent metasomatism, and/or multiple depletion events including source heterogeneity, although we do not have the resolution to quantify each factor precisely.

It is important to point out that the three harzburgite clinopyroxenes (SVF-9, -42 and -52) plot along the errorchron defined by lherzolite clinopyroxenes. Removing the three samples does not affect

the estimated errorchron age. The Lu/Hf ratio in orthopyroxene of spinel peridotite is expected to be higher than that of coexisting clinopyroxene (Eggins et al., 1998; Bedini and Bodinier, 1999; Witt-Eickchen and O'Neill, 2005), resulting in time-integrated growth of radiogenic Hf. If we assume that the Hf-isotopic equilibration between clinopyroxene and orthopyroxene in the harzburgites was fast enough, the $^{176}\text{Hf}/^{177}\text{Hf}$ ratios of the coexisting clinopyroxenes might be significantly elevated compared with those of the lherzolite clinopyroxenes – considering the orthopyroxene control for the Hf budget in harzburgite; but this is clearly not the case. The Lu–Hf isotopic compositions of the three harzburgite orthopyroxenes are thus expected to be falling along the errorchron defined by clinopyroxenes with higher values. That is, the Lu–Hf system seems to be unaffected by diffusional equilibration between pyroxenes. What we can say from our results is that the closure temperature for Lu and Hf diffusion in clinopyroxene of spinel peridotite might be quite high, on the order of ~ 900 °C or perhaps even higher.

6.2. Re–Os isotopic systematics

The Spitsbergen peridotites define generally positive correlations on the Re–Os isochron diagram (Fig. 6A), and Re vs. Al_2O_3 diagram (Fig. 4D). Sample SVF-36 with an extreme composition on the Re–Os isochron, contains carbonate-bearing pockets (Table 1), and has elevated Re concentration for its Al_2O_3 (Fig. 4D). The scattered data thus can be attributed to open-system behavior of Re during recent mantle metasomatism (e.g., Walker et al., 1989; Reisberg and Lorand, 1995; Carlson et al., 1999; Gao et al., 2002). However, while it is not possible to rule out some effect of metasomatism on the $^{187}\text{Os}/^{188}\text{Os}$ isotopic compositions, all samples possess sub-chondritic values (Fig. 6A) suggesting that such effects have been minimal. Even sample SVF-36 has sub-chondritic Os isotopic composition, suggesting that the elevated Re content was acquired only recently. The Os concentrations do not define a meaningful correlation with Al_2O_3 (Fig. S3C). The Os in spinel peridotites is considered to reside primarily in discrete sulfides (e.g., Shirey and Walker, 1998; Handler and Bennett, 1999; Burton et al., 2000). The Re also resides in a sulfide component in the spinel peridotite, with some control by clinopyroxene (Hart and Ravizza, 1996; Handler and Bennett, 1999; Burton et al., 2000). The scatter observed in Os concentrations (Fig. S3c) may simply reflect nugget effects caused by heterogeneous distribution of trace phases, possibly exsolved from monosulfide solid solutions during cooling (Handler and Bennett, 1999; Alard et al., 2002; Pearson et al., 2004). Meanwhile, $^{187}\text{Re}/^{188}\text{Os}$ ratios define a relatively good correlation with Al_2O_3 concentrations (Fig. S3D), except for sample SVF-36, further suggesting that Re and Os isotopic compositions have not been significantly disturbed by subsequent metasomatism. Our observation is reminiscent of a previous study by Handler and Bennett (1999) on peridotite xenoliths from S.E. Australia, in which PGEs and Re were not significantly mobilized during interaction with carbonate melts.

If the Re–Os isochron is forced through PUM, after excluding sample SVF-36 from the regression, the Spitsbergen peridotites yield an errorchron age of 2.1 ± 1.1 Ga, an initial γ_{Os} of $+0.2 \pm 3.6$ and an MSWD of 777 when the $\lambda^{187}\text{Re}$ value of $1.666 \times 10^{-11} \text{ yr}^{-1}$ (Shirey and Walker, 1998) is used in the calculation (Fig. 6A). We note that this apparent age is comparable to the independent estimates obtained from the Lu–Hf errorchron (Fig. 5B), even though there is a debate for the true value for PUM (Walker et al., 2002).

Further confirmation comes from determination of the Re-depletion age (T_{RD}) defined by Walker et al. (1989) This approach provides a model age to compare the Os isotopic composition of the xenolith at the time of host lava eruption to a primitive mantle growth model by assuming that the xenolith has no Re. If all of the Re was removed at the time of melting, then the T_{RD} age should equal the T_{MA} age. T_{RD} ages are always minimum ages. They provide good approximations for the time of melting in highly refractory perido-

tites, but severely underestimate the melting age of more fertile samples. The two most refractory samples analyzed for Re–Os isotopes, SVF-36 and SVF-41, which both contain less than 1% of Al_2O_3 , yield T_{RD} ages of 2.24 and 2.71 Ga, respectively (Table 3).

Alternatively, Re mobility can be overcome by plotting the Os isotopic compositions against an immobile element that exhibits a similar degree of incompatibility to Re during melting, such as Al_2O_3 , CaO, Y and HREE (Reisberg and Lorand, 1995; Handler et al., 1997). If the data display a positive correlation, then the $^{187}\text{Os}/^{188}\text{Os}$ of the y-intercept (Reisberg and Lorand, 1995) or the $^{187}\text{Os}/^{188}\text{Os}$ present at the lowest likely Al_2O_3 concentration (e.g., 0.7 wt.% Al_2O_3) (Handler et al., 1999) can be considered as the initial ratio. The time of melt depletion can be determined by comparing the initial ratio to a primitive mantle growth model. Spitsbergen samples display a relatively good correlation ($R^2 = 0.78$) in the Al_2O_3 vs. $^{187}\text{Os}/^{188}\text{Os}$ pseudo-isochron (alumina-chron) in Fig. 6B. The trend passes through the hypothetical PUM, suggesting that they reflect melt extraction processes from an essentially primitive mantle source. We also observe good trends between Os isotopic compositions and Mg# ($R^2 = 0.76$), CaO ($R^2 = 0.68$), and indicators of melt depletion such as Cr# in spinel ($R^2 = 0.60$) (Tables 1 and 2; Supplementary Table 2). Assuming that the correlation between $^{187}\text{Os}/^{188}\text{Os}$ and Al_2O_3 records a single melting event or series of melting events closely spaced in time, then the extrapolation of the pseudo-isochron to $\text{Al}_2\text{O}_3 \approx 0.6$ wt.% gives a model age of 2.2 ± 0.5 Ga (Fig. 6B), which is within error of the apparent ages defined by Lu–Hf and Re–Os isochrons above. Sample SVF-41, which is the most refractory and has the lowest Al_2O_3 (0.6 wt.%) – in fact falling below the lower limit (ca. 0.7 wt.%) at which it has been suggested Re/Os values approach zero during partial melting of the upper mantle (Handler et al., 1997) – has the highest Os concentration in the entire suite. This sample is characterized by a significantly lower $^{187}\text{Os}/^{188}\text{Os}$ value of 0.1096, defining a Neoproterozoic T_{RD} of 2.7 Ga, which is nearly equal to the T_{MA} age of 2.9 Ga (Table 3; Fig. 6B). The ages are supported by duplicate analyses (Table 3) of this sample. Collectively, the Paleoproterozoic/Neoproterozoic ages are confirmed by two independent methods. We thus interpret the computed age range as the time when this piece of mantle was accreted to the continental lithosphere beneath Spitsbergen.

6.3. Mantle–crust coupling and implications for the host basanite mantle source

It is generally acknowledged that the mean compositions of subcontinental lithospheric mantle sampled as xenoliths, garnet concentrates, and peridotite massifs have evolved from highly depleted Archean cratonic mantle to more fertile Phanerozoic mantle, probably associated with declining mantle temperature or a change in the mechanism of continental lithosphere generation or both (e.g., Boyd, 1989; Griffin et al., 1999, 2003; Pearson et al., 2004; Carlson et al., 2005). This evolution has been illustrated in a plot of olivine content against Mg# of olivine (Fig. 7), and a whole-rock Mg# against Cr# (Fig. S4). The fields of archon, proton and tecton, as defined by Griffin et al. (1999) (i.e., lithospheric mantle that experienced its last tectonothermal event at >2.5 Ga, 2.5–1.0 Ga, and <1.0 Ga, respectively, inferred from the age of the overlying crust) are shown for comparison in Fig. S4. Many xenoliths from Archean cratons are characterized by their higher Mg#s compared with off-cratonic samples, which may be related to a higher average degree of partial melting, possibly at greater depth. Spitsbergen peridotites are generally more depleted than the peridotites produced in Phanerozoic time, and plot in the field for hypothetical Proterozoic cratons. This result independently supports the Paleoproterozoic/Neoproterozoic ages determined with Lu–Hf and Re–Os systematics above.

Svalbard has been interpreted to have originated by amalgamation of several different terranes during large-scale transcurrent faulting in the waning stages of the Caledonian Orogeny (e.g., Harland, 1997;

Lyberis and Manby, 1999; Johansson et al., 2005). Based on comparison of pre-Caledonian and Caledonian tectonic histories, Svalbard can be subdivided into the western and eastern terranes along the Billefjorden Fault Zone (Fig. 1B) (e.g., Gee et al., 1994; Johansson et al., 2005). The western province of Svalbard is considered to be derived from northern Greenland or Ellesmere Island in the Canadian Arctic, whereas eastern Svalbard is thought to have originated from eastern Greenland (Fig. 1A) (Johansson et al., 2005, and references therein). The Paleoproterozoic/Neoproterozoic geological event has hitherto not been recognized in the western province of Svalbard. However, Bernard-Griffiths et al. (1993) showed that protoliths of eclogitic tectonic lenses in a Caledonian high-pressure metamorphic complex from central western Spitsbergen yield a mid-Paleoproterozoic age (igneous zircon; 2121 ± 50 Ma U–Pb zircon discordia upper interception age; Sm–Nd model age for the corresponding whole-rock sample = 2.17 Ga with $\varepsilon_{\text{Nd}(T)} = +5.2$). In northern Greenland and southeastern Ellesmere Island, Paleoproterozoic and Neoproterozoic gneiss complexes have been investigated by numerous conventional and SHRIMP zircon U–Pb age determinations together with whole-rock Sm–Nd isotopic analyses (Frisch, 1988; Frisch and Hunt, 1988; Nutman et al., 2008). Rough agreement between the ages for melt depletion of the Spitsbergen peridotites and the oldest crustal rock, suggests that stabilization of the lithospheric mantle beneath Spitsbergen may have been linked with formation of the overlying crust.

On the Sm–Nd isochron diagram (Fig. S2), the Spitsbergen peridotites define an errorchron age of 620 ± 260 Ma (2σ), an initial ε_{Nd} of $+9.8 \pm 6.1$ and a MSWD of 18. This may reflect partial resetting of the Sm–Nd system by the Caledonian orogeny, but we do not preclude simple mixing of residual radiogenic protolith with enriched metasomatizing agent(s). The metasomatic components are unlikely to be related with the host basalts, considering that (1) the host basalts have intermediate Sm–Nd isotopic compositions compared to the Spitsbergen peridotites (Fig. S2), and (2) the Lu–Hf isotopic composition of the host basanite falls off the trend defined by the peridotites on the Lu–Hf isochron plot (Fig. 5B). That is, the host basalts do not possess end-member isotopic characteristics. This finding is consistent with previous work for Sr–Nd isotopic systematics of the Spitsbergen peridotites and the host basalts (Ionov et al., 2002b).

Recently, Goldstein et al. (2008) showed that the western Gakkel Ridge volcanism was derived from an enriched mantle with Dupal-like

characteristics, and that the Spitsbergen host basalts form an enriched end-member for the Gakkel basalts on Sr–Nd–Pb isotopic diagrams. The authors argued that the Svalbard lithospheric mantle might have been delaminated, and dispersed into the convecting Arctic asthenosphere during the separation of Svalbard and Greenland, resulting in formation of an enriched component with a Dupal-like signature. This idea supposes that the host basaltic volcanism originated by partial melting of the Spitsbergen lithospheric mantle. We present here some evidence which refutes this idea. First, we note that the host basanite has a Hf isotopic composition that is coupled to its Nd isotopic composition, therefore plotting along the mantle array, within the field for oceanic island basalts on the Nd–Hf isotopic plot (Fig. 5A). This is distinctly different from the peridotite xenoliths which exhibit significant Nd–Hf decoupling, even when we consider only the weighted mean ($^{143}\text{Nd}/^{144}\text{Nd} = 0.51309 \pm 0.00015$, and $^{176}\text{Hf}/^{177}\text{Hf} = 0.28420 \pm 0.00062$) of the measured values.

Furthermore, the host basanite has considerably less radiogenic Hf isotopic compositions than any of the peridotite xenoliths (Fig. 5A). This observation implies that a genetic relationship between the xenoliths and the host basaltic volcanism is weak at best. In fact, the host basalts display less radiogenic $^{208}\text{Pb}/^{204}\text{Pb}$ ratios than the Spitsbergen xenoliths at a given $^{207}\text{Pb}/^{204}\text{Pb}$ ratio on the $^{208}\text{Pb}/^{204}\text{Pb}$ vs. $^{207}\text{Pb}/^{204}\text{Pb}$ diagram (Fig. 4 in Ionov et al., 2002b), which further supports our notion. Most importantly, the Re–Os and Lu–Hf age data we have presented here suggest that the ancient Paleoproterozoic/Neoproterozoic lithospheric mantle persists beneath western Spitsbergen despite the tectono-magmatic reactivation and change in tectonic regimes from transpressive to transtensive since the Paleocene (e.g., Tuchschild and Spillmann, 1992; Ljones et al., 2004). It should be stressed that there is no meaningful correlation between temperature and whole-rock compositions or isotopic compositions for the Spitsbergen samples (Tables 1–3; Supplementary Tables 2 and 3), which implies that the lithospheric mantle is not stratified with respect to composition, and that the ancient fragments are not relics preserved locally at relatively shallow depth. These lines of evidence suggest that it is unlikely for detached and recycled bulk portions of the lithospheric mantle beneath the Svalbard Archipelago to have become the enriched source for the western Gakkel Ridge volcanism.

If we simply define 'lithospheric thickness' as the depth where the geotherm intersects the mantle adiabat (~ 1280 °C) – although its definition is somewhat arbitrary – lithospheric thickness derived from the xenoliths-defined Spitsbergen geotherm (Amundsen et al., 1987) is estimated to be about 25 kbar, corresponding to a thickness of ~ 85 km. The samples we have studied are estimated to have originated at depths equivalent to ~ 7 to 11 kbar of pressure. This may leave a potential for deeper portion of the lithosphere to be delaminated or mechanically eroded during extension of the Lena Trough and become the enriched magma source in the shallow convecting mantle. Although our understanding of the nature of lithospheric root is not yet crystal clear, we may expect, if any, the deepest lithospheric mantle beneath Spitsbergen to have relatively little contrast in geochemistry compared to the asthenosphere. If this is the case, input of deeper part of the lithospheric mantle to the Arctic magma sources is hard to identify. Furthermore, it is unreasonable to expect lateral variation of the magma sources with distance from the continental margin. Overall, the evidence does not support reactivated subcontinental lithospheric mantle (SCLM) as the prevalent enriched end-member for the Dupal-like signature in the Arctic Ocean Basin.

Recent Re–Os studies have shown that some abyssal peridotites record melting events older than the age of the ridge they are dredged from, on spatial scales of individual sulfide grains within a single sample or even in bulk-rock analyses (Brandon et al., 2000; Harvey et al., 2006; Liu et al., 2008). These inherited, ancient partial melting effects have also been reported in peridotites brought to the surface by lavas in the Hawaiian plume, in forearc peridotites, and in ophiolites (Parkinson et al., 1998; Bizimis et al., 2007; Pearson et al.,

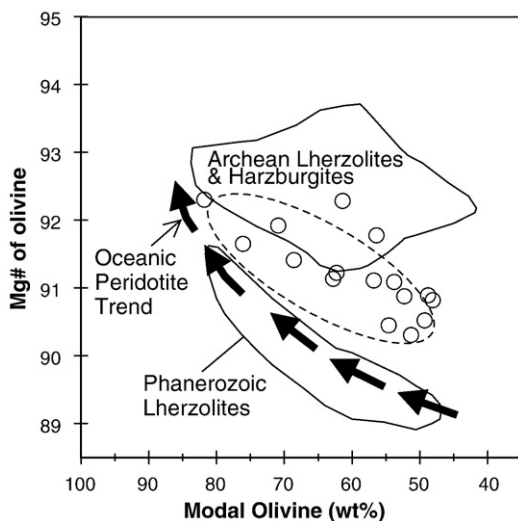


Fig. 7. Modal weight percent vs. Mg# ($= 100 \text{ Mg}/(\text{Mg} + \text{Fe})$) of olivine from Spitsbergen peridotites. Data sources: fields of Archean Lherzolites and harzburgites, and Phanerozoic Lherzolites from Griffin et al. (1999); oceanic peridotite trend from Boyd (1989).

2007), which were taken as evidence for a heterogeneous upper mantle. The refractory nature of the melt-depleted peridotites – that is its higher solidus temperature than fertile mantle – might result in long-term survival in the convecting mantle (Harvey et al., 2006; Bizimis et al., 2007; Liu et al., 2008), although much work is needed in the future in order to fully understand the isolation mechanism. This observation raises an issue that the correlation observed in the Spitsbergen peridotites (Fig. 6B) may represent simple mixing between relatively fertile and ancient, refractory mantle preserved in the convecting mantle for billions of years. For this to be the case, some assumptions are necessary, such as that (1) the peridotites have been only recently emplaced at lithospheric depths (ca. 840–1020 °C/7–11 kbar), and (2) a significant amount of lithospheric erosion occurred before the emplacement at current levels. However, there is no available seismological data to support this model yet. Furthermore, we note that the Paleoproterozoic/Neoproterozoic age has been independently supported by the Lu–Hf systematics and geochemistry of the peridotites. We thus interpret it as the lithospheric mantle formation age beneath Spitsbergen. Combined Lu–Hf and Re–Os isotope systematics are therefore required to adequately estimate the stabilization age of the lithospheric mantle.

7. Conclusions

- (1) The Paleoproterozoic/Neoproterozoic age of SCLM incorporation in Spitsbergen has been confirmed by several independent methods: Lu–Hf and Re–Os isotopic systematics, and geochemistry of the peridotite xenoliths.
- (2) The long-term survival of the SCLM, despite protracted tectonomagmatic reactivation in this area, argues against delaminated mantle lithosphere as a significant source of geochemically enriched mantle components in the Arctic region.
- (3) The Lu–Hf system can be used to date mantle melting events recorded in peridotite xenoliths, in combination with the Re–Os system.
- (4) Carbonate-rich metasomatic melts have severely impacted the Sm–Nd system of the Spitsbergen residual peridotites, but not the Lu–Hf and Re–Os systematics. It remains to be demonstrated whether these relationships are universal in mantle domains that have undergone carbonate metasomatism.
- (5) Clinopyroxene grains from Spitsbergen peridotite are characterized by strong Nd–Hf decoupling on isotopic correlation diagrams, whereas the host basanite plots within the field for oceanic basalts. The host basanite volcanism is not likely to have been derived by partial melting of the Spitsbergen lithospheric mantle.

Acknowledgements

Funding for this project has come from Polar Academic Program (PAP), Korea Polar Research Institute to SHC. This work was supported in part by Grant-in-Aid from JSPS to KS. Insightful reviews by Laurie Reisberg and John Lassiter greatly improved the manuscript. We would like to thank B.K. Park, K.H. Kim, Y.J. Jwa, M. Kusakabe, K. Nagao, and S.B. Park for their assistance with field work in 2007, and A.V. Andronikov, C. Stefano, H. Yamamoto, M.K. Choo, and J.U. Seo for assistance with analytical work.

Appendix A. Supplementary data

Supplementary data associated with this article can be found, in the online version, at doi:10.1016/j.epsl.2010.06.013.

References

Alard, O., Griffin, W.L., Lorand, J.P., Jackson, S.E., O'Reilly, S.Y., 2000. Non-chondritic distribution of the highly siderophile elements in mantle sulphides. *Nature* 407, 891–894.

- Alard, O., Griffin, W.L., Pearson, N.J., Lorand, J.-P., O'Reilly, S.Y., 2002. New insights into the Re–Os systematics of sub-continental lithospheric mantle from in situ analysis of sulphides. *Earth Planet. Sci. Lett.* 203, 651–663.
- Alard, O., Luguet, A., Pearson, N.J., Griffin, W.L., Lorand, J.-P., Gannoun, A., Burton, K.W., O'Reilly, S.Y., 2005. In situ Os isotopes in abyssal peridotites bridge the isotopic gap between MORBs and their source mantle. *Nature* 436, 1005–1008.
- Amundsen, H.E.F., 1987. Evidence for liquid immiscibility in the upper mantle. *Nature* 327, 692–695.
- Amundsen, H.E.F., Griffin, W.L., O'Reilly, S.Y., 1987. The lower crust and upper mantle beneath northwestern Spitsbergen: evidence from xenoliths and geophysics. *Tectonophysics* 139, 169–185.
- Andres, M., Blichert-Toft, J., Schilling, J., 2004. Nature of the depleted upper mantle beneath the Atlantic: evidence from Hf isotopes in normal mid-ocean ridge basalts from 79°N to 55°S. *Earth Planet. Sci. Lett.* 225, 89–103.
- Bedini, R.M., Bodinier, J.-L., 1999. Distribution of incompatible trace elements between the constituent of spinel peridotite xenoliths: ICP-MS data from the East African Rift. *Geochim. Cosmochim. Acta* 63, 3883–3900.
- Bernard-Griffiths, J., Peucat, J.J., Ohta, Y., 1993. Age and nature of protoliths in the Caledonian blueschist–eclogite complex of western Spitsbergen: a combined approach using U–Pb, Sm–Nd and REE whole-rock systems. *Lithos* 30, 81–90.
- Bernstein, S., Kelemen, P.B., Brooks, C.K., 1998. Depleted spinel harzburgite xenoliths in Tertiary dykes from East Greenland: restites from high degree melting. *Earth Planet. Sci. Lett.* 154, 221–235.
- Bizimis, M., Sen, G., Salters, V.J.M., 2003. Hf–Nd isotope decoupling in the oceanic lithosphere: constraints from spinel peridotites from Oahu, Hawaii. *Earth Planet. Sci. Lett.* 217, 43–58.
- Bizimis, M., Griselin, M., Lassiter, J.C., Salters, V.J.M., Sen, G., 2007. Ancient recycled mantle lithosphere in the Hawaiian plume: Osmium–hafnium isotopic evidence from peridotite mantle xenoliths. *Earth Planet. Sci. Lett.* 257, 259–273.
- Blichert-Toft, J., Albarède, F., 1997. The Lu–Hf isotope geochemistry of chondrites and the evolution of the mantle–crust system. *Earth Planet. Sci. Lett.* 148, 243–258.
- Blichert-Toft, J., Albarède, F., Kornprobst, J., 1999. Lu–Hf isotope systematics of garnet pyroxenites from Beni Bousera, Morocco: implications for basalt origin. *Science* 283, 1303–1306.
- Blichert-Toft, J., Agrani, A., Andres, M., Kingsley, R., Schilling, J., Albarède, F., 2005. Geochemical segmentation of the Mid-Atlantic Ridge north of Iceland and ridge-hot spot interaction in the North Atlantic. *Geochim. Geophys. Geosyst.* 6, 1–27.
- Blythe, A.E., Kleinspehn, K.L., 1998. Tectonically versus climatically driven exhumation of the Eurasian plate margin, Svalbard: fission track analyses. *Tectonics* 17, 621–639.
- Boyd, F.R., 1989. Compositional distinction between oceanic and cratonic lithosphere. *Earth Planet. Sci. Lett.* 96, 15–26.
- Brandon, A.D., Snow, J.E., Walker, R.J., Morgan, J.W., Mock, T.D., 2000. ¹⁹⁰Pt–¹⁸⁶Os and ¹⁸⁷Re–¹⁸⁷Os systematics of abyssal peridotites. *Earth Planet. Sci. Lett.* 177, 319–335.
- Burton, K.W., Schiano, P., Birck, J.-L., Allègre, C.J., Rehkämper, M., Halliday, A.N., Dawson, J.B., 2000. The distribution and behaviour of rhenium and osmium amongst mantle minerals and the age of the lithospheric mantle beneath Tanzania. *Earth Planet. Sci. Lett.* 183, 93–106.
- Carlson, R.W., Pearson, D.G., Boyd, F.R., Shirey, S.B., Irvine, G., Menzies, A.H., Gurney, J.J., 1999. Re–Os systematic of lithospheric peridotites: implications for lithosphere formation and preservation. In: Gurney, J.L., Pascoe, M.D., Richardson, S.H. (Eds.), *The J.B. Dawson volume, Proceedings of the VIIth International Kimberlite Conference*. Red Roof Design, Cape Town, pp. 99–108.
- Carlson, R.W., Irving, A.J., Schulze, D.J., Carter Hearn Jr, B., 2004. Timing of Precambrian melt depletion and Phanerozoic refertilization events in the lithospheric mantle of the Wyoming Craton and adjacent Central Plains Orogen. *Lithos* 77, 453–472.
- Carlson, R.W., Pearson, D.G., James, D.E., 2005. Physical, chemical, and chronological characteristics of continental mantle. *Rev. Geophys.* 43, 1–24.
- Chauvel, C., Blichert-Toft, J., 2001. A hafnium isotope and trace element perspective on melting of the depleted mantle. *Earth Planet. Sci. Lett.* 190, 137–151.
- Choi, S.H., Mukasa, S.B., Andronikov, A.V., Osanai, Y., Harley, S.L., Kelly, N.M., 2006. Lu–Hf systematics of the ultra-high temperature Napier metamorphic complex in Antarctica: evidence for the early Archean differentiation of Earth's mantle. *Earth Planet. Sci. Lett.* 246, 305–316.
- Choi, S.H., Mukasa, S.B., Zhou, X.-H., Xian, X.H., Andronikov, A.V., 2008. Mantle dynamics beneath East Asia constrained by Sr, Nd, Pb and Hf isotopic systematics of ultramafic xenoliths and their host basalts from Hannuoba, North China. *Chem. Geol.* 248, 40–61.
- Crane, K., Eldholm, O., Myhre, A.M., Sundvor, E., 1982. Thermal implications for the evolution of the Spitsbergen transform fault. *Tectonophysics* 89, 1–32.
- Eggins, S.M., Rudnick, R.L., McDonough, W.F., 1998. The composition of peridotites and their minerals: a laser-ablation ICP-MS study. *Earth Planet. Sci. Lett.* 154, 53–71.
- Eldholm, O., Myhre, A.M., Thiede, J., 1994. Cenozoic tectono-magmatic events in the North Atlantic: potential paleo environmental implications. In: Boulter, M.C., Fischer, H.C. (Eds.), *Cenozoic Plants and Climates of the Arctic: NATO ASI Ser.* 127. Springer-Verlag, Heidelberg, pp. 35–55.
- Feden, R.H., Vogt, P.R., Flemming, H.S., 1979. Magnetic and bathymetric evidence for the “Yermak hot spot” northwest of Svalbard in the Arctic basin. *Earth Planet. Sci. Lett.* 44, 18–38.
- Frey, F.A., Green, D.H., 1974. The mineralogy, geochemistry and origin of Iherzolite inclusion in Victorian basanites. *Geochim. Cosmochim. Acta* 38, 1023–1059.
- Frisch, T., 1988. Reconnaissance geology of the Precambrian Shield of Ellesmere, Devon and Coburg islands, Canadian Arctic Archipelago. *Geol. Surv. Can. Mem.* 409 102 pp. + 4 maps.
- Frisch, T., Hunt, P.A., 1988. U–Pb zircon and monazite ages from the Precambrian Shield of Ellesmere and Devon islands, Arctic Archipelago. *Geol. Surv. Can. Pap.* 88–2, 117–125.

- Gao, S., Rudnick, R.L., Carlson, R.W., McDonough, W.F., Liu, Y.-S., 2002. Re–Os evidence for replacement of ancient mantle lithosphere beneath the North China craton. *Earth Planet. Sci. Lett.* 198, 307–322.
- Gee, D.G., Björklund, L., Stölen, L.-K., 1994. Early Proterozoic basement in Ny Friesland – implications for the Caledonian tectonics of Svalbard. *Tectonophysics* 231, 171–182.
- Goldstein, S.L., Soffer, G., Langmuir, C.H., Lehner, K.A., Graham, D.W., Michael, P.J., 2008. Origin of a 'Southern Hemisphere' geochemical signature in the Arctic upper mantle. *Nature* 453, 89–93.
- Griffin, W.L., O'Reilly, S.Y., Ryan, C.G., 1999. The composition and origin of sub-continental lithospheric mantle. In: Fei, Y., Bertka, C.M., Mysen, B.O. (Eds.), *Mantle Petrology; Field Observation and High Pressure Experimentation – A Tribute to Francis R (Joe) Boyd*: *Geochem. Soc. Spec. Publ.*, vol. 6, pp. 13–45.
- Griffin, W.L., Pearson, N.J., Belousova, E., Jackson, S.E., O'Reilly, S.Y., van Achterberg, E., Shee, S.R., 2000. The Hf isotope composition of cratonic mantle: LAM-MC-ICPMS analysis of zircon megacrysts in kimberlites. *Geochim. Cosmochim. Acta* 64, 133–147.
- Griffin, W.L., O'Reilly, S.Y., Abe, N., Aulbach, S., Davies, R.M., Pearson, N.J., Doyle, B.J., Kivi, K., 2003. The origin and evolution of Archean lithospheric mantle. *Precambrian Res.* 127, 19–41.
- Hanan, B.B., Blichert-Toft, J., Pyle, D.G., Christie, D.M., 2004. Contrasting origins of the upper mantle revealed by hafnium and lead isotopes from the Southeast Indian Ridge. *Nature* 432, 91–94.
- Handler, M.R., Bennett, V.C., 1999. Behaviour of platinum-group elements in the subcontinental mantle of eastern Australia during variable metasomatism and melt depletion. *Geochim. Cosmochim. Acta* 63, 3597–3618.
- Handler, M.R., Bennett, V.C., Esat, T.M., 1997. The persistence of off-cratonic lithospheric mantle: Os isotopic systematics of variably metasomatized southeast Australian xenoliths. *Earth Planet. Sci. Lett.* 151, 61–75.
- Handler, M.R., Bennett, V.C., Dreibus, G., 1999. Evidence from correlated Ir/Os and Cu/S for late-stage Os mobility in peridotite xenoliths: implications for Re–Os systematics. *Geology* 27, 75–78.
- Hanghøj, K., Kelemen, P., Bernstein, S., Blusztajn, J., Frei, R., 2001. Osmium isotopes in the Wiedemann Fjord mantle xenoliths: a unique record of cratonic mantle formation by melt depletion in the Archean. *Geochim. Geophys. Geosyst.* 2 2000GC000085.
- Harland, W.B., 1969. Contribution of Spitsbergen to understanding of tectonic evolution of North Atlantic region. In: Kay, M. (Ed.), *North Atlantic: Geology and Continental Drift*, 12. American Association of Petroleum Geologists, Tulsa, OK, Memoir, pp. 817–851.
- Harland, W.B., 1997. The geology of Svalbard. *Geol. Soc. London, Mem.* vol. 17 521 pp.
- Hart, S.R., Ravizza, G.E., 1996. Os partitioning between phases in lherzolite and basalt. In: Basu, A., Hart, S.R. (Eds.), *Earth Processes: Reading the Isotopic Code*: *Am. Geophys. Union, Geophys. Monogr.*, vol. 95, pp. 123–134.
- Harvey, J., Gannoun, A., Burton, K.W., Rogers, N.W., Alard, O., Parkinson, I.J., 2006. Ancient melt extraction from the oceanic upper mantle revealed by Re–Os isotopes in abyssal peridotites from the Mid-Atlantic ridge. *Earth Planet. Sci. Lett.* 244, 606–621.
- Hellebrand, E., Snow, J.E., 2003. Deep melting and sodic metasomatism underneath the highly oblique-spreading Lena Trough (Arctic Ocean). *Earth Planet. Sci. Lett.* 216, 283–299.
- Ionov, D.A., 1998. Trace element composition of mantle-derived carbonates and coexisting phases in peridotite xenoliths from Kalki basalts. *J. Petrol.* 39, 1931–1941.
- Ionov, D.A., Dupuy, C., O'Reilly, S.Y., Kopylova, M.G., Genshaft, Y.S., 1993. Carbonated peridotite xenoliths from Spitsbergen: implications for trace element signature of mantle carbonate metasomatism. *Earth Planet. Sci. Lett.* 119, 283–297.
- Ionov, D.A., O'Reilly, S.Y., Genshaft, Y.S., Kopylova, M.G., 1996. Carbonate-bearing mantle peridotite xenoliths from Spitsbergen: phase relationships, mineral compositions and trace-element residence. *Contrib. Mineral. Petrol.* 125, 375–392.
- Ionov, D.A., Bodinier, J.-L., Mukasa, S.B., Zanetti, A., 2002a. Mechanisms and sources of mantle metasomatism: major and trace element compositions of peridotite xenoliths from Spitsbergen in the context of numerical modeling. *J. Petrol.* 43, 2219–2259.
- Ionov, D.A., Mukasa, S.B., Bodinier, J.-L., 2002b. Sr–Nd–Pb isotopic compositions of peridotite xenoliths from Spitsbergen: numerical modeling indicates Sr–Nd decoupling in the mantle by melt percolation metasomatism. *J. Petrol.* 43, 2261–2278.
- Johansson, Å., Gee, D.G., Larionov, A.N., Ohta, Y., Tebenkov, A.M., 2005. Grenvillian and Caledonian evolution of eastern Svalbard – a tale of two orogenies. *Terra Nova* 17, 317–325.
- Jung, H., Mo, W., Choi, S.H., 2009. Deformation microstructures of olivine in peridotite from Spitsbergen, Svalbard and implications for seismic anisotropy. *J. Metamorphic Geol.* 27, 707–720.
- Kato, Y., Fujinaga, K., Suzuki, K., 2005. Major and trace element geochemistry and Os isotopic composition of metalliferous umbers from the late Cretaceous Japanese accretionary complex. *Geochem. Geophys. Geosyst.* 6 2005GC000920.
- Liu, C.-Z., Snow, J.E., Hellebrand, E., Brüggemann, G., von der Handt, A., Büchl, A., Hofmann, A.W., 2008. Ancient, highly heterogeneous mantle beneath Gakkel ridge, Arctic Ocean. *Nature* 452, 311–316.
- Ljones, F., Kuwano, A., Mjelde, R., Breivik, A., Shimanura, H., Murai, Y., Nishimura, Y., 2004. Crustal transect from the North Atlantic Knipovich Ridge to the Svalbard margin west of Hornsund. *Tectonophysics* 378, 17–41.
- Lyberis, N., Manby, G., 1999. Continental collision and lateral escape deformation in the lower and upper crust: an example from Caledonide Svalbard. *Tectonics* 18, 40–63.
- Maaløe, A., Aoki, K., 1977. The major element composition of the upper mantle estimated from the composition of lherzolites. *Contrib. Mineral. Petrol.* 63, 161–173.
- McDonough, W.F., 1990. Constraints on the composition of the continental lithospheric mantle. *Earth Planet. Sci. Lett.* 101, 1–18.
- McDonough, W.F., Sun, S.-S., 1995. The composition of the Earth. *Chem. Geol.* 120, 223–253.
- Meisel, T., Walker, R.J., Irving, A.J., Lorand, J.-P., 2001. Osmium isotopic compositions of mantle xenoliths: a global perspective. *Geochim. Cosmochim. Acta* 65, 1311–1323.
- Nowell, G.M., Kempton, P.D., Noble, S.R., Fitton, J.G., Saunders, A.D., Mahoney, J.J., Taylor, R.N., 1998. High precision Hf isotope measurements of MORB and OIB by thermal ionization mass spectrometry: insights into the depleted mantle. *Chem. Geol.* 149, 211–233.
- Nutman, A.P., Dawes, P.R., Kalsbeek, F., Hamilton, M.A., 2008. Paleoproterozoic and Archaean gneiss complexes in northern Greenland: Paleoproterozoic terrane assembly in the High Arctic. *Precambrian Res.* 161, 419–451.
- Palme, H., Nickel, K.G., 1985. Ca/Al ratio and compositions of the Earth's upper mantle. *Geochim. Cosmochim. Acta* 49, 2123–2132.
- Parkinson, I.J., Hawkesworth, C.J., Cohen, A.S., 1998. Ancient mantle in a modern arc: osmium isotopes in Izu–Bonin–Mariana forearc peridotites. *Science* 281, 2011–2013.
- Pearson, D.G., Nowell, G.M., 2003. Dating mantle differentiation: a comparison of the Lu–Hf, Re–Os and Sm–Nd isotope systems in the Beni Bousera peridotite massif and constraints on the Nd–Hf composition of the lithospheric mantle. *Geophys. Res. Abst.* 5, 05430.
- Pearson, N.J., Alard, O., Griffin, W.L., Jackson, S.E., O'Reilly, S.Y., 2002. In situ measurement of Re–Os isotopes in mantle sulfides by laser ablation multi-collector-inductively coupled plasma mass spectrometry: analytical methods and preliminary results. *Geochim. Cosmochim. Acta* 66, 1037–1050.
- Pearson, D.G., Irvine, G.J., Ionov, D.A., Boyd, F.R., Dreibus, G.E., 2004. Re–Os isotope systematics and platinum group element fractionation during mantle melt extraction: a study of massif and xenolith peridotite suites. *Chem. Geol.* 208, 29–59.
- Pearson, D.G., Parman, S.W., Nowell, G.M., 2007. A link between large mantle melting events and continent growth seen in osmium isotopes. *Nature* 449, 202–205.
- Rampono, E., Bottazzi, P., Ottolini, L., 1991. Complementary Ti and Zr anomalies in orthopyroxene and clinopyroxene from mantle peridotites. *Nature* 354, 518–520.
- Reisberg, L., Lorand, J.-P., 1995. Longevity of sub-continental mantle lithosphere from osmium isotope systematics in orogenic peridotite massifs. *Nature* 376, 159–162.
- Salters, V.J.M., 1996. The generation of mid-ocean ridge basalts from the Hf and Nd isotope perspective. *Earth Planet. Sci. Lett.* 141, 109–123.
- Salters, V.J.M., White, W.M., 1998. Hf isotope constraint on mantle evolution. *Chem. Geol.* 145, 447–460.
- Scherer, E.E., Münker, C., Mezger, K., 2001. Calibration of the lutetium–hafnium clock. *Science* 293, 683–687.
- Shirey, S.B., Walker, R.J., 1998. The Re–Os isotope system in cosmochemistry and high-temperature geochemistry. *Annu. Rev. Earth Planet. Sci.* 26, 423–500.
- Skjeltvåle, B.-L., Amundsen, H.E.F., O'Reilly, S.Y., Griffin, W.L., Gjelsvik, T., 1989. A primitive alkali basaltic stratovolcano and associated eruptive centres, Northwestern Spitsbergen: volcanology and tectonic significance. *J. Volcanol. Geotherm. Res.* 37, 1–19.
- Snow, J.E., Reisberg, L., 1995. Os isotopic systematic of the MORB mantle: results from altered abyssal peridotites. *Earth Planet. Sci. Lett.* 133, 411–421.
- Sun, S.-S., McDonough, W.F., 1989. Chemical and isotopic systematic of oceanic basalts: implications for mantle composition and processes. *Geol. Soc. London. Spec. Publ.* 42, 313–345.
- Suzuki, K., Miyata, Y., Kanazawa, N., 2004. Precise Re isotope ratio measurements by negative thermal ionization mass spectrometry (N-TIMS) using total evaporation technique. *Int. J. Mass Spectrom.* 235, 97–101.
- Talwani, M., Eldhom, O., 1977. Evolution of the Norwegian–Greenland Sea. *Geol. Soc. Am. Bull.* 88, 969–999.
- Tuchschild, M., Spillmann, P., 1992. Neogene and Quaternary volcanism on Spitsbergen – the rival of an Arctic hot spot. *Schweiz. Mineral. Petrogr. Mitt.* 72, 251–270.
- Vervoort, J.D., Blichert-Toft, J., 1999. Evolution of the depleted mantle: Hf isotope evidence from juvenile rocks through time. *Geochim. Cosmochim. Acta* 63, 533–556.
- Vogt, P.R., Feden, R.H., Eldholm, O., Sundvor, E., 1978. The ocean crust west and north of the Svalbard Archipelago, synthesis and new results. *Polarforschung* 48, 1–19.
- Walker, R.J., Carlson, R.W., Shirey, S.B., Boyd, F.R., 1989. Os, Sr, Nd, and Pb isotopic systematics of southern African peridotite xenoliths implications for the chemical evolution of the subcontinental mantle. *Geochim. Cosmochim. Acta* 53, 1583–1595.
- Walker, R.J., Prichard, H.M., Ishiwatari, A., Pimentel, M., 2002. The osmium isotopic composition of convecting upper mantle deduced from ophiolite chromites. *Geochim. Cosmochim. Acta* 66, 329–345.
- Wells, P.R.A., 1977. Pyroxene thermometry in simple and complex systems. *Contrib. Mineral. Petrol.* 62, 129–139.
- Witt-Eickchen, G., O'Neill, H.St.C., 2005. The effect of temperature on the equilibrium distribution of trace elements between clinopyroxene, orthopyroxene, olivine and spinel in upper mantle peridotite. *Chem. Geol.* 221, 65–101.
- Witt-Eickchen, G., Seck, H.A., 1991. Solubility of Ca and Al in orthopyroxene from spinel peridotite: an improved version of an empirical geothermometer. *Contrib. Mineral. Petrol.* 106, 431–439.
- Wittig, N., Baker, J.A., Downes, H., 2007. U–Th–Pb and Lu–Hf isotopic constraints on the evolution of sub-continental lithospheric mantle, French Massif Central. *Geochim. Cosmochim. Acta* 71, 1290–1311.